Journal of Coordination Chemistry
Publication details, including instructions for authors and subscription information:
http://www.tandfonline.com/loi/gcoo20

Synthesis, characterization, and properties of copper and manganese complexes with 5-(benzimidazol-1-ylmethyl)isophthalate

Hai-Wei Kuai [a], Taka-Aki Okamura [b] & Wei-Yin Sun [a]

[a] State Key Laboratory of Coordination Chemistry, Coordination Chemistry Institute, School of Chemistry and Chemical Engineering, Nanjing National Laboratory of Microstructures, Nanjing University, Nanjing 210093, China

[b] Department of Macromolecular Science, Graduate School of Science, Osaka University, Toyonaka, Osaka 560-0043, Japan

Accepted author version posted online: 16 Jul 2012.Published online: 27 Jul 2012.

To cite this article: Hai-Wei Kuai, Taka-Aki Okamura & Wei-Yin Sun (2012) Synthesis, characterization, and properties of copper and manganese complexes with 5-(benzimidazol-1-ylmethyl)isophthalate, Journal of Coordination Chemistry, 65:18, 3147-3159, DOI: 10.1080/00958972.2012.712116

To link to this article: http://dx.doi.org/10.1080/00958972.2012.712116

Journal of Coordination Chemistry
Vol. 65, No. 18, 20 September 2012, 3147–3159

Synthesis, characterization, and properties of copper and manganese complexes with 5-(benzimidazol-1-ylmethyl)isophthalate

HAI-WEI KUAI†, TAKA-AKI OKAMURA‡ and WEI-YIN SUN*†

†State Key Laboratory of Coordination Chemistry, Coordination Chemistry Institute, School of Chemistry and Chemical Engineering, Nanjing National Laboratory of Microstructures, Nanjing University, Nanjing 210093, China
‡Department of Macromolecular Science, Graduate School of Science, Osaka University, Toyonaka, Osaka 560-0043, Japan

(*Received 19 April 2012; in final form 2 July 2012*)

Four new complexes, [Cu(L)] (**1**), $[Cu_2(L)(dpe)_{0.5}]\cdot 2.5H_2O$ (**2**), [Mn(L)] (**3**), and [Mn(L)(pybim)] (**4**) [H_2L = 5-(benzimidazol-1-ylmethyl)isophthalic acid, dpe = 1,2-di(pyridin-4-yl)ethylene, pybim = 2-(pyridin-2-yl)-1H-benzimidazole], have been synthesized under hydrothermal conditions and characterized by single-crystal and powder X-ray diffractions, FT-IR, and elemental analysis. The crystal structural analyses reveal that **1** and **4** are uninodal 3-connected 2-fold interpenetrated 2-D networks with (6^3) topology, **2** shows an infinite 1-D double-stranded chain structure, and **3** exhibits a uninodal 4-connected 2-D network with ($4^4\cdot 6^2$) topology. The factors influencing the structures of the coordination polymers are discussed. In addition, the thermal stabilities of **1**–**4**, second-order non-linear optical effect of **1,** and preliminary magnetic property of **3** have also been investigated.

Keywords: Copper and manganese complexes; Crystal structure; Metal–organic frameworks; NLO effect

1. Introduction

The crystal engineering of metal–organic frameworks (MOFs) has received attention because of their intriguing structures, topologies, and potential applications in magnetism, optical materials, catalysis, molecular/ionic recognition, and adsorption [1]. Typically, construction of MOFs involves interconnections of metal centers and bridging ligands to generate overall architectures, which can be influenced by factors such as the nature of metal ions and ligands, auxiliary ligands, and reaction conditions [2]. Structures and properties of the resultant coordination complexes may be closely related to the intrinsic features of ligands [3]. Therefore, the design of ligands becomes extremely important in this field. Among the well-employed organic ligands, N- and/or

*Corresponding author. Email: sunwy@nju.edu.cn

ISSN 0095-8972 print/ISSN 1029-0389 online © 2012 Taylor & Francis
http://dx.doi.org/10.1080/00958972.2012.712116

O-donor multi-dentate ligands are excellent building blocks for construction of desirable frameworks. However, compared with other N- and/or O-donor ligands, those containing both sterically hindered N-donors such as benzimidazolyl and carboxylate may exhibit distinctive features and induce new structural evolution, which may be helpful in the exploration of new crystalline materials and the study of correlation between the reaction conditions and structures of resultant complexes [4].

Recently, we have focused our attention on utilization of benzimidazol-1-yl and carboxylate-containing 5-(benzimidazol-1-ylmethyl)isophthalic acid (H_2L) as a building block for construction of coordination polymers with desirable structures and properties. The arene-cored H_2L exhibits a great advantage over other N- and/or O-donors since it possesses two functional groups, carboxylate, and sterically hindered benzimidazol-1-yl groups. Due to different coordination of carboxylates such as $\mu_1-\eta^1:\eta^0$-monodentate, $\mu_1-\eta^1:\eta^1$-chelating and $\mu_2-\eta^1:\eta^1$-bridging modes, H_2L can act as a multi-connector in assembly of complexes with diverse structures. Metal centers may also be expected to be bridged by carboxylates to mediate magnetic interactions [5]. The sterically hindered benzimidazolyl group may induce new structural evolution and maintain a specific coordination configuration [6]. As an aromatic dicarboxylate, L^{2-} can act as a bridging rod. The effect of steric hindrance of benzimidazolyl is important in the assembly process. Herein, we report preparation and characterization of four coordination polymers, [Cu(L)] (**1**), $[Cu_2(L)(dpe)_{0.5}]\cdot 2.5H_2O$ (**2**), [Mn(L)] (**3**), and [Mn(L)(pybim)] (**4**) [dpe = 1,2-di(pyridin-4-yl)ethylene, pybim = 2-(pyridin-2-yl)-1H-benzimidazole]. The influence of auxiliary ligands, steric hindrance of ligands, and solvent on the structures of coordination polymers will be discussed. Thermal stabilities of **1**–**4**, second-order non-linear optical (NLO) effect of **1**, and preliminary magnetic property of **3** have also been investigated.

2. Experimental

2.1. *Materials and methods*

All commercially available chemicals and solvents are of reagent grade and used as received. According to the literature [7], a slight revised experimental procedure was used to prepare the H_2L. Elemental analyses of C, H, and N were taken on a Perkin-Elmer 240C elemental analyzer at the analysis center of Nanjing University. The content of metal in complexes was determined by measurements of inductively coupled plasma (ICP) on a J-A1100 (Jarrell-Ash, USA) ICP spectrometer. Infrared spectra (IR) were recorded on a Bruker Vector22 FT-IR spectrophotometer by using KBr pellets. Thermogravimetric analyses (TGA) were performed on a simultaneous SDT 2960 thermal analyzer under nitrogen with a heating rate of $10^\circ C\,min^{-1}$. Powder X-ray diffraction (PXRD) patterns were measured on a Shimadzu XRD-6000 X-ray diffractometer with Cu-Kα ($\lambda = 1.5418$ Å) radiation at room temperature. The second-order NLO intensity was estimated by measuring a powder sample of 80–150 μm diameter in the form of a pellet relative to urea. A pulsed Q-switched Nd:YAG laser at a wavelength of 1064 nm was used to generate a second-harmonic-generation (SHG) signal from powder samples. The backscattered SHG light was collected by a spherical concave mirror and passed through a filter that transmits only

532 nm radiation. The magnetic measurement in the temperature range 1.8–300 K was carried out on a Quantum Design MPMS7 SQUID magnetometer in a field of 2000 Oe. Diamagnetic corrections were made using Pascal's constants.

2.2. *Synthesis*

2.2.1. Synthesis of [Cu(L)] (1). Reaction mixture of $Cu(NO_3)_2 \cdot 3H_2O$ (24.1 mg, 0.1 mmol), H_2L (29.6 mg, 0.1 mmol), 2 mL ethanol, and NaOH (8.0 mg, 0.2 mmol) in 12 mL of water was sealed in a 16 mL Teflon-lined stainless steel container and heated at 180°C for 3 days. After cooling to room temperature, dark-green platelet crystals of **1** were collected by filtration and washed by water and ethanol several times with a yield of 32%. Anal. Calcd for $C_{16}H_{10}N_2O_4Cu$ (%): C, 53.71; H, 2.82; N, 7.83; Cu, 17.76. Found (%): C, 53.56; H, 2.62; N, 7.59; Cu, 17.60. IR (KBr pellet, cm^{-1}): 1622 (s), 1589 (m), 1517 (s), 1470 (s), 1428 (s), 1394 (m), 1356 (s), 1297 (w), 1255 (w), 1234 (w), 1196 (m), 1124 (w), 1107 (w), 980 (w), 934 (w), 900 (w), 816 (w), 752 (s), 735 (s), 592 (w), 478 (w).

2.2.2. Synthesis of $[Cu_2(L)(dpe)_{0.5}] \cdot 2.5H_2O$ (2). Reaction mixture of $Cu(NO_3)_2 \cdot 3H_2O$ (24.1 mg, 0.1 mmol), H_2L (29.6 mg, 0.1 mmol), dpe (18.2 mg, 0.1 mmol), 2 mL ethanol, and NaOH (8.0 mg, 0.2 mmol) in 12 mL of water was sealed in a 16 mL Teflon-lined stainless steel container and heated at 180°C for 3 days. After cooling to room temperature, yellow block crystals of **2** were collected by filtration and washed by water and ethanol several times with a yield of 36% based on H_2L. Anal. Calcd for $C_{44}H_{40}N_6O_{13}Cu_4$ (%): C, 47.40; H, 3.62; N, 7.54; Cu, 22.82. Found (%): C, 47.26; H, 3.42; N, 7.59; Cu, 22.54. IR (KBr pellet, cm^{-1}): 3425 (m), 1613 (s), 1576 (s), 1512 (w), 1432 (w), 1398 (m), 1343 (s), 1297 (m), 1267 (m), 1234 (m), 1208 (m), 1187 (m), 1154 (w), 1102 (m), 980 (w), 841 (w), 748 (s), 638 (m), 613 (m), 554 (m), 431 (m).

2.2.3. Synthesis of [Mn(L)] (3). A mixture of $MnCl_2 \cdot 4H_2O$ (19.8 mg, 0.1 mmol), H_2L (29.6 mg, 0.1 mmol), and NaOH (8.0 mg, 0.2 mmol) in 12 mL of water was stirred for 10 min in air, and then transferred to a 16 mL Teflon-lined stainless steel container and heated at 180°C for 3 days. After cooling to room temperature, colorless block crystals of **3** were collected by filtration and washed by water and ethanol several times with a yield of 36%. Anal. Calcd for $C_{16}H_{10}N_2O_4Mn$ (%): C, 55.03; H, 2.89; N, 8.02; Mn, 15.73. Found (%): C, 54.86; H, 2.99; N, 7.89; Mn, 15.56. IR (KBr pellet, cm^{-1}): 1621 (s), 1569 (s), 1545 (s), 1509 (s), 1453 (s), 1382 (s), 1291 (w), 1241 (w), 1185 (m), 1130 (w), 1104 (w), 967 (w), 912 (w), 871 (w), 806 (w), 775 (m), 760 (s), 740 (s), 725 (s), 679 (w), 649 (w), 593 (w), 527 (w).

2.2.4. Synthesis of [Mn(L)(pybim)] (4). Reaction mixture of $MnCl_2 \cdot 4H_2O$ (19.8 mg, 0.1 mmol), H_2L (29.6 mg, 0.1 mmol), pybim (19.5 mg, 0.1 mmol), and NaOH (8.0 mg, 0.2 mmol) in 10 mL H_2O was sealed in a 16 mL Teflon-lined stainless steel container and heated at 180°C for 3 days. After cooling to room temperature, pale yellow crystals of **4** were isolated by filtration and washed by water and ethanol several times in 42% yield based on H_2L. Anal. Calcd for $C_{28}H_{19}N_5O_4Mn$ (%): C, 61.77; H, 3.52; N, 12.86; Mn,

10.09. Found (%): C, 62.02; H, 3.80; N, 12.66; Mn, 10.32. IR (KBr pellet, cm^{-1}): 1624 (s), 1593 (s), 1537 (s), 1500 (m), 1457 (s), 1414 (s), 1383 (m), 1345 (s), 1290 (m), 1234 (m), 1197 (w), 1148 (w), 974 (m), 900 (w), 801 (m), 758 (s), 708 (s), 690 (m), 567 (w), 424 (m).

2.3. *X-ray crystallography*

The X-ray diffraction data for **1** were collected on a Rigaku Rapid II imaging plate area detector with Mo-Kα radiation ($\lambda = 0.71075$ Å) using MicroMax-007HF microfocus rotating anode X-ray generator and VariMax-Mo optics at 200 K. The structure of **1** was solved by direct methods with *SIR*92 [8] and expanded using Fourier techniques [9]. Crystallographic data collections for **2**–**4** were carried out on a Bruker Smart Apex CCD area-detector diffractometer using graphite-monochromated Mo-Kα radiation ($\lambda = 0.71073$ Å) at 293 K. The diffraction data were integrated using the SAINT program [10], which was also used for intensity corrections for Lorentz and polarization effects. Semi-empirical absorption correction was applied using SADABS [11]. The structures were solved by direct methods and all non-hydrogen atoms were refined anisotropically on F^2 by full-matrix least-squares using the SHELXL-97 crystallographic software package [12]. In **1**–**4**, all hydrogen atoms attached to carbon were generated geometrically; hydrogen atoms in O5 in **2** and N3 in **4** were found at reasonable positions in the difference Fourier maps and located there; part of the hydrogen atoms in lattice water of **2** could not be located and thus were not included in refinement. Details of crystal parameters, data collection, and refinements for the complexes are summarized in table 1. Selected bond lengths and angles of **1**–**4** are listed in table 2.

Table 1. Crystallographic data and structure refinement details for **1**–**4**.

	1	**2**	**3**	**4**
Empirical formula	$C_{16}H_{10}N_2O_4Cu$	$C_{44}H_{40}N_6O_{13}Cu_4$	$C_{16}H_{10}N_2O_4Mn$	$C_{28}H_{19}N_5O_4Mn$
Formula weight	357.80	1114.98	349.20	544.42
Temperature (K)	200	293(2)	293(2)	293(2)
Crystal system	Monoclinic	Monoclinic	Monoclinic	Monoclinic
Space group	*Pc*	$P2_1/c$	$P2_1/c$	$P2_1/c$
Unit cell dimensions (Å, °)				
a	6.697(6)	7.078(5)	8.2678(17)	15.1916(19)
b	8.639(8)	27.526(5)	11.577(2)	10.7173(14)
c	11.398(11)	11.604(5)	17.036(3)	15.777(2)
β	90.93(4)	102.393(5)	119.033(7)	114.051(2)
Volume ($Å^3$), *Z*	659.3(10), 2	2208.1(19), 2	1425.7(5), 4	2345.6(5), 4
Calculated density ($g\,cm^{-3}$)	1.802	1.677	1.627	1.542
F(000)	362	1132	708	1116
θ range (°)	3.04–25.00	1.94–28.00	2.23–27.81	2.37–27.71
Reflections collected	4670	13,762	8739	14,808
Independent reflections on F^2	2140	5260	3314	5429
Goodness-of-fit	1.179	1.049	0.906	1.032
R_1 [$I > 2\sigma(I)$][a]	0.0687	0.0588	0.0340	0.0539
wR_2 [$I > 2\sigma(I)$][b]	0.1835	0.1781	0.0626	0.1208

[a] $R_1 = \Sigma||F_o| - |F_c||/\Sigma|F_o|$, [b] $wR_2 = |\Sigma w(|F_o|^2 - |F_c|^2)|/\Sigma|w(F_o)^2|^{1/2}$, where $w = 1/[\sigma^2(F_o^2) + (aP)^2 + bP]$; $P = (F_o^2 + 2F_c^2)/3$.

3. Results and discussion

3.1. *Preparation*

Complexes **1**–**4** were obtained under hydrothermal conditions at 180°C. NaOH was used as alkaline reagent to neutralize the carboxylic acid. Reduction of Cu(II) to Cu(I) occurred in formation of **2** as reported previously [13]. In addition, it was found that **2** can only be obtained in the water–ethanol system although several systems such as water, water–methanol, water–DMF, and water–acetonitrile have been tried. This implies that the solvent can subtly influence formation of coordination polymers. Complexes **1**–**4** are stable in air in the solid state.

3.2. *Structural description*

3.2.1. Crystal structure of [Cu(L)] (1). The structural analysis shows that **1** crystallizes in monoclinic acentric space group *Pc* with Flack parameter of −0.02(3). As exhibited

Table 2. Selected bond lengths (Å) and angles (°) for **1**–**4**

1			
Cu(1)–N(12)	1.933(8)	Cu(1)–O(1)#1	1.893(7)
Cu(1)–O(3)#2	1.978(6)	Cu(1)–O(4)#2	2.014(6)
O(1)#1–Cu(1)–N(12)	101.8(3)	O(3)#2–Cu(1)–N(12)	94.2(3)
O(4)#2–Cu(1)–N(12)	159.7(2)	O(1)#1–Cu(1)–O(3)#2	164.0(3)
O(1)#1–Cu(1)–O(4)#2	98.6(3)	O(3)#2–Cu(1)–O(4)#2	65.5(3)
2			
Cu(1)–O(1)	1.831(3)	Cu(1)–N(3)	1.870(4)
Cu(2)–N(11)	1.863(4)	Cu(2)–O(3)#1	1.866(3)
O(1)–Cu(1)–N(3)	171.82(19)	O(3)#1–Cu(2)–N(11)	175.23(19)
3			
Mn(1)–O(1)	2.1836(16)	Mn(1)–O(2)	2.2201(15)
Mn(1)–O(4)#1	2.0699(15)	Mn(1)–N(12)#2	2.1366(17)
Mn(1)–O(3)#3	2.0807(14)		
O(1)–Mn(1)–O(2)	59.10(5)	O(1)–Mn(1)–O(4)#1	130.50(6)
O(1)–Mn(1)–N(12)#2	110.11(7)	O(1)–Mn(1)–O(3)#3	97.56(6)
O(2)–Mn(1)–O(4)#1	89.80(6)	O(2)–Mn(1)–N(12)#2	101.50(7)
O(2)–Mn(1)–O(3)#3	156.12(6)	O(4)#1–Mn(1)–N(12)#2	113.48(6)
O(3)#3–Mn(1)–O(4)#1	103.97(6)	O(3)#3–Mn(1)–N(12)#2	90.91(6)
4			
Mn(1)–O(1)	2.066(2)	Mn(1)–N(1)	2.497(3)
Mn(1)–N(2)	2.197(3)	Mn(1)–N(12)#1	2.188(3)
Mn(1)–O(3)#2	2.152(2)	Mn(1)–O(4)#2	2.468(2)
O(1)–Mn(1)–N(1)	161.52(9)	O(1)–Mn(1)–N(2)	92.24(10)
O(1)–Mn(1)–N(12)#1	95.71(10)	O(1)–Mn(1)–O(3)#2	116.61(9)
O(1)–Mn(1)–O(4)#2	102.40(9)	N(1)–Mn(1)–N(2)	70.35(10)
N(1)–Mn(1)–N(12)#1	85.70(10)	O(3)#2–Mn(1)–N(1)	81.78(9)
O(4)#2–Mn(1)–N(1)	86.01(9)	N(2)–Mn(1)–N(12)#1	112.26(10)
O(3)#2–Mn(1)–N(2)	142.25(10)	O(4)#2–Mn(1)–N(2)	95.93(9)
O(3)#2–Mn(1)–N(12)#1	89.75(9)	O(4)#2–Mn(1)–N(12)#1	145.78(8)
O(3)#2–Mn(1)–O(4)#2	56.19(8)		

Symmetry transformations used to generate equivalent atoms: For **1**, #1 $x, y, 1+z$; #2 $-1+x, 2-y, 1/2+z$; for **2**, #1 $-1+x, y, -1+z$; for **3**, #1 $-x, 1/2+y, 3/2-z$; #2 $-x, 1-y, 1-z$; #3 $x, 3/2-y, -1/2+z$; for **4**, #1 $x, -1+y, z$; #2 $x, 1/2-y, 1/2+z$.

in figure 1(a), there are one Cu(II) ion and one L^{2-} ligand in the asymmetrical unit of **1**. Each Cu(II) is four-coordinate by one nitrogen atom from benzimidazolyl of one L^{2-} ligand and three carboxylate oxygen atoms from another two different L^{2-} ligands to furnish distorted square-planar coordination. Thus the Cu(II) center can be regarded as a 3-connected node. Each L^{2-} is a μ_3-connector using its two carboxylates with $\mu_1-\eta^1:\eta^0$-monodentate and $\mu_1-\eta^1:\eta^1$-chelating coordination, respectively (scheme 1) and benzimidazolyl. Infinite interconnection of metals and L^{2-} leads to formation of a 2-D structural motif (figure 1b). From the perspective view of topology, if each Cu(II) and L^{2-} is treated as a node, the structure of **1** can be simplified into a uninodal 3-connected 2-D network (figure 1c). The flexible 2-D networks of **1** twist and distort to some extent to interpenetrate each other. Thus **1** can be described as a uninodal 3-connected 2-fold interpenetrated 2-D net with (6^3) topology (figure S1).

3.2.2. Crystal structure of $[Cu_2(L)(dpe)_{0.5}]\cdot 2.5H_2O$ (2). When dpe was introduced into the reaction system as an auxiliary ligand, **2** was obtained. It crystallizes in the monoclinic $P2_1/c$ space group. As shown in figure 2(a), the asymmetric unit of **2** consists of two crystallographically independent Cu(I), one L^{2-} ligand, half of dpe, and two and a half lattice water molecules. Each Cu(I) in **2** is two-coordinate with a carboxylate oxygen and a nitrogen atom from benzimidazolyl of L^{2-} or dpe to generate a nearly linear coordination geometry. An infinite 1-D chain is formed *via* interconnection of Cu2 and L^{2-}, which is further linked by dpe to give a 1-D neutral double-stranded chain (figure 2b). Apart from the coordination, hydrogen-bonding interactions stabilize resultant solid-state structure. According to their function in constructing the supramolecule, we divide the hydrogen bonds into two groups: (1) O5–H16···O2#1 and C18–H10···O5. These interactions link adjacent double-stranded chains to form a 2-D network (figures S2a and S2b) and (2) C12-H6···O4#2. Hydrogen bonds further connect 2-D layers leading to a 3-D supramolecular structure (figures S2c and S2d). The hydrogen-bonding data for **2** are summarized in table S1.

3.2.3. Crystal structure of [Mn(L)] (3). Complex **3** crystallizes in the monoclinic $P2_1/c$ space group with an asymmetric unit of **3** composed of one Mn(II) ion and one L^{2-} ligand. As shown in figure 3(a), each Mn(II) is five-coordinate with NO_4 donor set by one benzimidazolyl nitrogen atom from one L^{2-} ligand and four carboxylate oxygen atoms from another three different L^{2-} ligands to furnish a distorted square-pyramidal coordination geometry. The equatorial plane is defined by four oxygen atoms with mean deviation of 0.24 Å; Mn(II) deviates 0.49 Å from this plane toward the apex. One carboxylate of L^{2-} in **3** adopts $\mu_1-\eta^1:\eta^1$-chelating coordination, while the other one exhibits $\mu_2-\eta^1:\eta^1$-bridging mode (scheme 1) with Mn–O bond lengths of 2.0699(15) and 2.0807(14) Å (table 1). Two Mn(II) are linked by two $\mu_2-\eta^1:\eta^1$-bridging carboxylates to form a $[Mn_2(COO)_2]$ sub-unit with Mn···Mn distance of 3.96 Å, indicating that there might be weak magnetic interactions within binuclear units (vide post). In **3**, each L^{2-} bridges four different Mn(II)'s and each Mn(II) is coordinated by four different L^{2-} ligands. This linkage infinitely extends to form a 2-D network (figure 3b). The topology for both Mn(II) and L^{2-} can be regarded as 4-connecting nodes. As a result, **3** can be simplified into a uninodal (4,4)-connected 2-D **sql** network with the point (Schläfli) symbol of ($4^4.6^2$) (figure 3c).

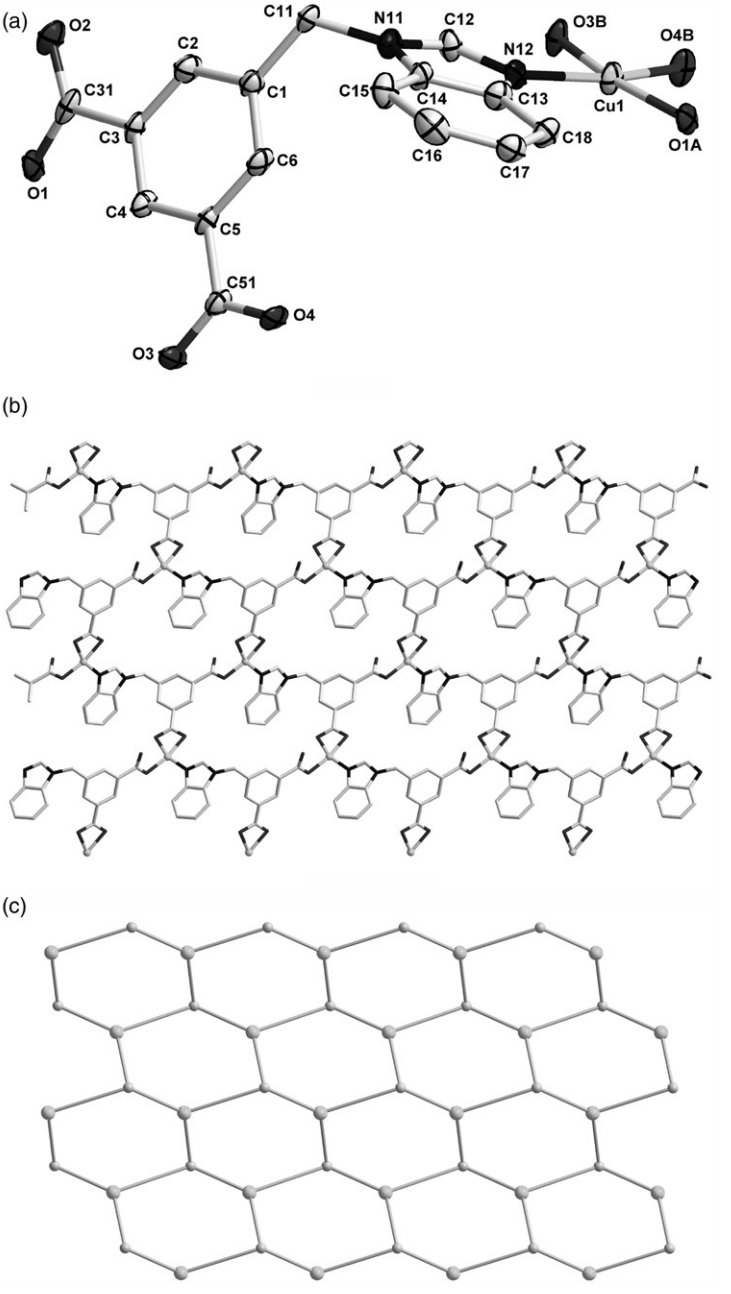

Figure 1. (a) The coordination environment of Cu(II) in **1** with ellipsoids drawn at the 30% probability level. Hydrogen atoms are omitted for clarity. Symmetry codes: A, x, y, $1+z$; B, $-1+x$, $2-y$, $1/2+z$. (b) 2-D network of **1**. (c) Schematic representation of the uninodal 3-connected 2-D network with (6^3) topology of **1**.

3.2.4. Crystal structure of [Mn(L)(pybim)] (4). Single-crystal X-ray diffraction analysis revealed that **4** is also in the monoclinic $P2_1/c$ space group. The asymmetric unit of **4** contains one Mn(II) ion, one L^{2-} ligand, and one pybim. Each Mn(II) with N_3O_3 donor

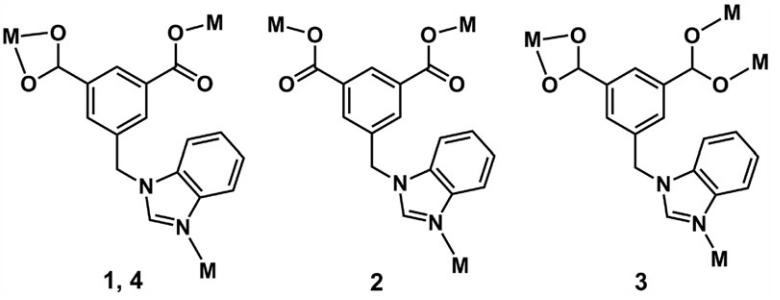

Scheme 1. Coordination modes of L^{2-} in **1–4**.

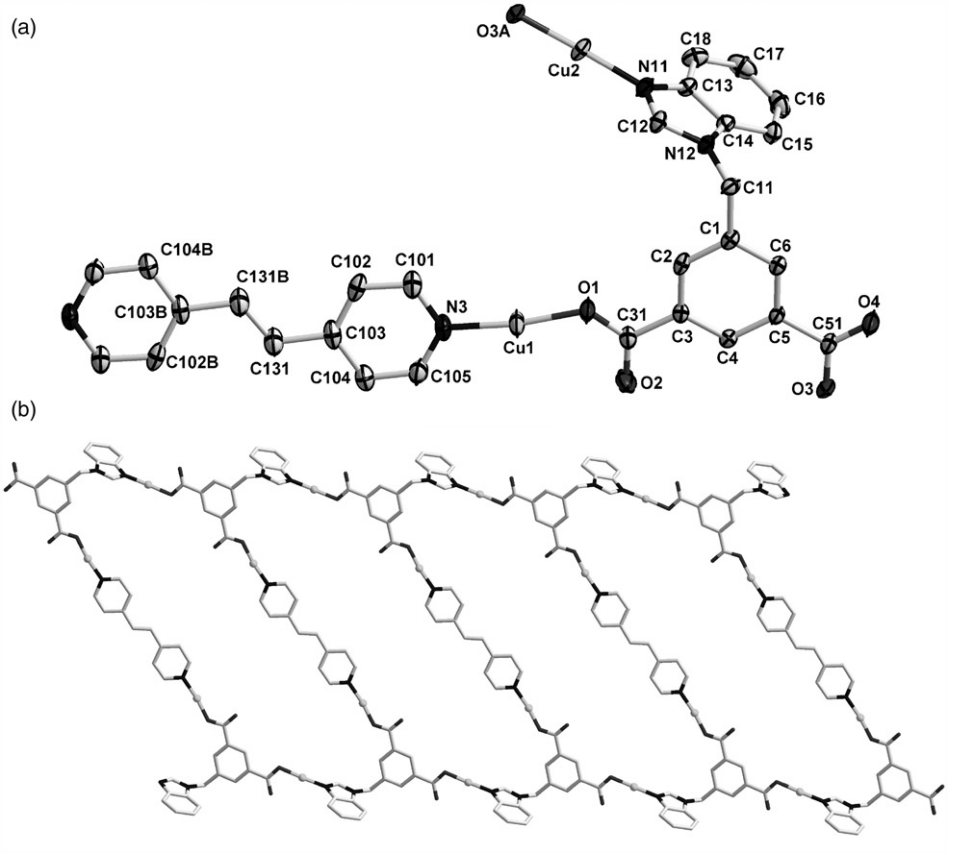

Figure 2. (a) The coordination environment of Cu(I) in **2** with ellipsoids drawn at the 30% probability level. Hydrogen atoms and lattice water molecules are omitted for clarity. Symmetry codes: A, $-1+x$, y, $-1+z$. (b) The 1-D chain of **2**.

set is six-coordinate by three carboxylate oxygen atoms from two different L^{2-} ligands, two nitrogen atoms from coordinated pybim, and one nitrogen atom from benzimidazolyl of L^{2-} with heavily distorted octahedral coordination geometry (figure 4a). The equatorial plane is composed of two carboxylate oxygen atoms, one

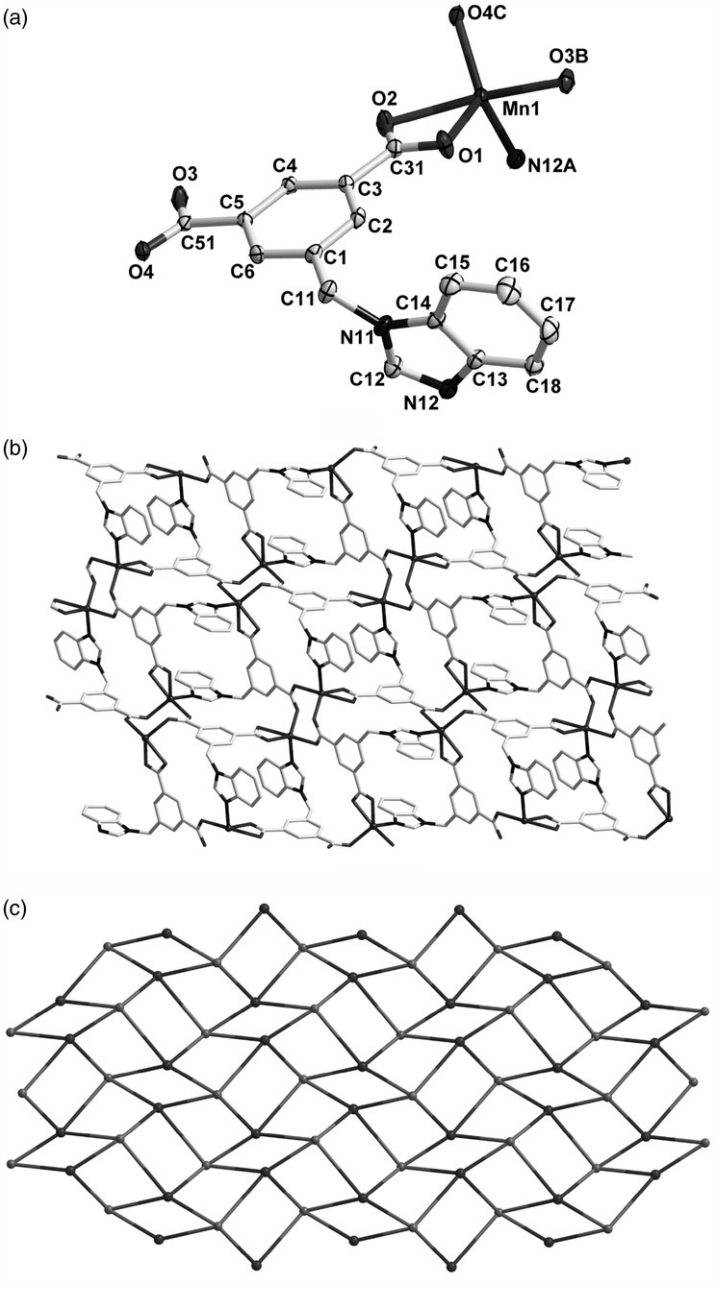

Figure 3. (a) The coordination environment of Mn(II) in **3** with 30% probability. Hydrogen atoms were omitted for clarity. Symmetry codes: A, $-x$, $1-y$, $1-z$; B, x, $3/2-y$, $-1/2+z$; C, $-x$, $1/2+y$, $3/2-z$. (b) 2-D network of **3**. (c) Schematic representation of the uninodal 4-connected 2-D network of **3** with $(4^4 \cdot 6^2)$ topology.

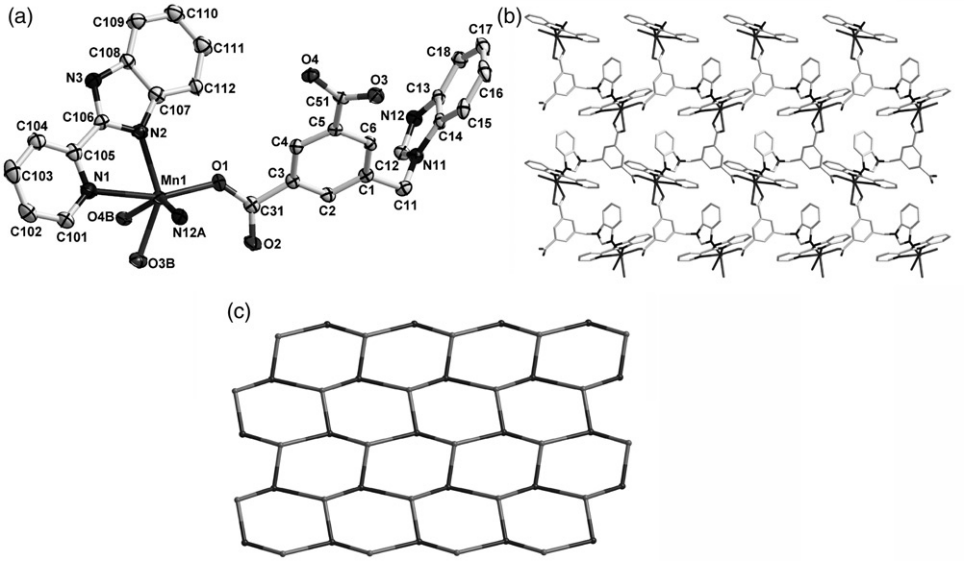

Figure 4. (a) The coordination environment of Mn(II) in **4** with 30% probability. Hydrogen atoms were omitted for clarity. Symmetry codes: A, $x, -1+y, z$; B, $x, 1/2-y, 1/2+z$. (b) 2-D network of **4**. (c) Schematic representation of the uninodal 3-connected 2-D network of **4** with (6^3) topology.

benzimidazolyl nitrogen atom, and one nitrogen from pybim; the axial positions are one carboxylate oxygen and nitrogen of pybim. One carboxylate of L^{2-} in **4** adopts $\mu_1-\eta^1:\eta^0$-monodentate coordination while the other one is $\mu_1-\eta^1:\eta^0$-chelating (scheme 1). In **4,** each L^{2-} bridges three different Mn(II) ions and in turn each Mn(II) is coordinated by three different L^{2-} ligands. This connection extends infinitely to form a 2-D network (figure 4b). Both L^{2-} and Mn(II) in **4** can be regarded as 3-connectors, Thus the network of **4** can be simplified into a uninodal 3-connected 2-D network with the point (Schläfli) symbol of (6^3) (figure 4c).

3.2.5. Structural comparison of 1–4. Complexes **1**–**4** have diverse architectures from 1-D chain to 2-D networks with different topologies (vide supra). The different structures of **1** and **2** as well as **3** and **4** can be ascribed to the effect of auxiliary ligand since the other experimental conditions are the same. The difference between **1** and **3** is caused by the different centers with different coordination number and geometry. Both **1** and **4** are 2-D networks with the same (6^3) topology; however, **1** shows a 2-fold interpenetration, while no interpenetration was found in **4**, perhaps due to steric hindrance of pybim.

3.3. *PXRD, IR, and TGA*

The pure phases of **1**–**4** were confirmed by PXRD measurements. As shown in figure S3, each PXRD pattern of the as-synthesized sample is consistent with the simulated one.

Complete deprotonation of H_2L to give L^{2-} in **1**–**4** was confirmed by crystal structures and IR spectral data (see section 2) since no characteristic vibrations for −COOH between 1680 and 1760 cm^{-1} were observed [14].

Complexes **1**–**4** were subjected to TGA under nitrogen to ascertain their thermal stability from 30°C to 660°C (figure S4). In the TGA curves of **1**, **3**, and **4**, no obvious weight loss was observed before decomposition of frameworks at *ca* 283°C for **1**, 538°C for **3**, and 428°C for **4**, confirming no solvent in the architectures of these complexes. For **2**, a weight loss of 8.1% from 72°C to 156°C is assigned to release of lattice water molecules (Calcd 8.1%), and the decomposition of the residue was observed at 270°C.

3.4. *NLO property of 1*

Non-centrosymmetric structures may have second-order NLO effect [14, 15]. Complex **1** crystallizes in the acentric space group *Pc* which belongs to the polar point group C_3^2. Therefore, the optical properties were investigated to evaluate potential applications as second-order NLO materials. Approximate estimations were carried out on a pulsed Q-switched Nd:YAG laser at a wavelength of 1064 nm. The result obtained from a powdered sample (80–150 μm diameters) as a pellet (Kurtz powder test) was compared with those obtained for urea. The preliminary experimental results revealed that **1** exhibits modest powder SHG intensity compared to that for urea with a response of 0.8 times.

3.5. *Magnetic property of 3*

In **3**, two Mn(II) ions are bridged by carboxylates to form a dinuclear $[Mn_2(COO)_2]$ with Mn···Mn distance of 3.96 Å, which may mediate magnetic interactions [16]. Therefore, the magnetism of **3** was investigated from 1.8 to 300 K with a 2000 Oe applied magnetic field. The magnetic behavior of **3** in the form of χ_M, χ_M^{-1}, and $\chi_M T$ *versus* T are depicted in figure 5. The $\chi_M T$ value of 5.52 emu K mol^{-1} at 300 K is higher than the value expected for magnetically isolated Mn(II) (4.38 emu K mol^{-1}, $g = 2.0$), suggesting the existence of magnetic interactions between neighboring Mn(II) centers. As the temperature is gradually lowered, the $\chi_M T$ value decreases continuously with an extrapolated value which vanishes when T approaches 0; the χ_M value increases smoothly to reach 0.179 emu mol^{-1} at 1.8 K. The χ_M^{-1} value (above 28 K) obeys the Curie–Weiss law with a Weiss constant (θ) of −18.36 K and a Curie constant (C) of 3.06 emu K mol^{-1}. The negative value for θ confirms antiferromagnetic interactions between neighboring Mn(II) centers [17].

4. Conclusion

Hydrothermal reactions of the semi-rigid H_2L with copper and manganese salts at 180°C in the presence/absence of N-donor auxiliary ligands provide four coordination polymers. Complex **1** shows a uninodal 3-connected 2-fold interpenetrated 2-D network with (6^3) topology; **2** has a 1-D double-stranded chain structure, which can be extended to 3-D supramolecular net by hydrogen-bonding; **3** exhibits a uninodal 4-connected 2-D

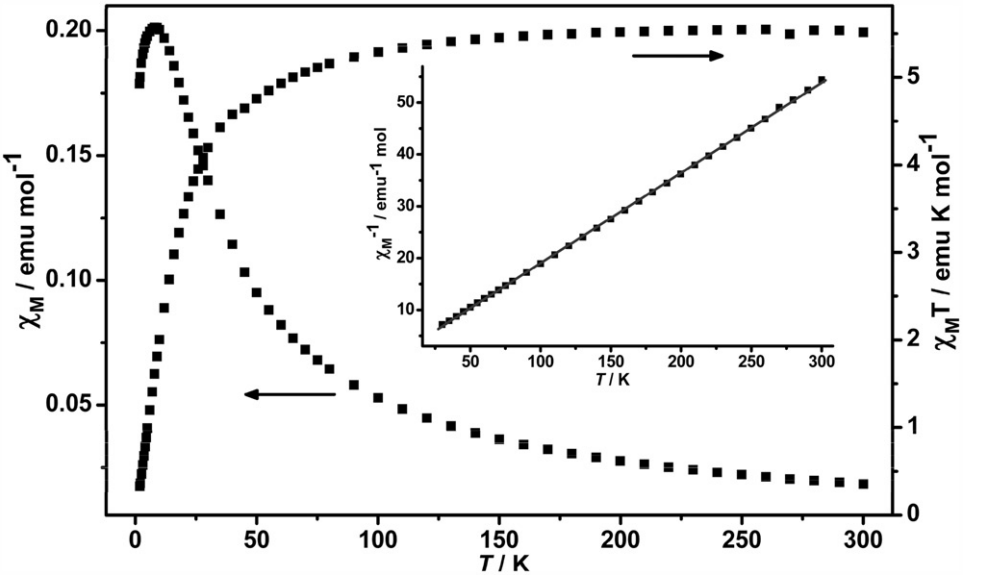

Figure 5. Temperature dependences of magnetic susceptibility of χ_M, χ_M^{-1}, and $\chi_M T$ for **3**. The solid line represents the fitted curve.

network with $(4^4 \cdot 6^2)$ topology; **4** displays a uninodal 3-connected 2-D network with (6^3) topology. The results of this study not only imply that steric hindrance and auxiliary ligands play an important role in construction of coordination polymers, but also afford a good example of solvent controlled polymeric architecture, as previously reported copper and manganese coordination polymers with benzenedicarboxylate ligands [18].

Supplementary material

Crystallographic data for the structures reported in this article have been deposited with the Cambridge Crystallographic Data Centre as Supplementary Publication Nos CCDC-876693 (**1**), 876694 (**2**), 869284 (**3**), and 869285 (**4**). Copies of the data can be obtained at http://www.ccdc.cam.ac.uk/conts/retrieving.html (or from the CCDC, 12 Union Road, Cambridge CB2 1EZ, UK; Fax:+44 1223336033; E-mail: deposit@ccdc.cam.ac.uk).

Acknowledgments

This work was financially supported by the National Natural Science Foundation of China (Grant nos 91122001 and 21021062) and the National Basic Research Program of China (Grant no. 2010CB923303).

References

[1] (a) Y. Liu, K. Li, S.C. Wei, M. Pan, C.Y. Su. *CrystEngComm*, **13**, 4564 (2011); (b) X.L. Wang, C. Qin, E.B. Wang, L. Xu, Z.M. Su, C.W. Hu. *Angew. Chem., Int. Ed.*, **43**, 5036 (2004); (c) Z. Su, M. Chen, T. Okamura, M.S. Chen, S.S. Chen, W.Y. Sun. *Inorg. Chem.*, **50**, 985 (2011); (d) L.J. Li, G. Yuan, L. Chen, D.Y. Du, X.L. Wang, G.J. Xu, H.N. Wang, K.Z. Shao, Z.M. Su. *J. Coord. Chem.*, **64**, 1578 (2011); (e) B. Liu, L.J. Fan, Y.Y. Liu, J. Yang, J.F. Ma. *J. Coord. Chem.*, **64**, 413 (2011).

[2] (a) K. Biradha, C.Y. Su, J.J. Vittal. *Cryst. Growth Des.*, **11**, 875 (2011); (b) Q.Y. Yang, K. Li, J. Luo, M. Pan, C.Y. Su. *Chem. Commun.*, **47**, 4234 (2011); (c) J.A. Zhang, M. Pan, J.J. Jiang, Z.G. She, Z.J. Fan, C.Y. Su. *Inorg. Chim. Acta*, **374**, 269 (2011); (d) L. Tang, Y.P. Wu, F. Fu, P. Zhang, N. Wang, L.F. Gao. *J. Coord. Chem.*, **63**, 1873 (2010).

[3] (a) Q. Yuan, K. Cai, Z.P. Qi, Z.S. Bai, Z. Su, W.Y. Sun. *J. Inorg. Biochem.*, **103**, 1156 (2009); (b) Z.S. Bai, Z.P. Qi, Y. Lu, Q. Yuan, W.Y. Sun. *Cryst. Growth Des.*, **8**, 1924 (2008); (c) S.S Chen, M. Chen, Takamizawa, M.S. Chen, Z.Su, W.Y. Sun. *Chem. Commun.*, **47**, 752 (2011); (d) S.S. Chen, M. Chen, Takamizawa, P. Wang, G.C. Lv, W.Y. Sun. *Chem. Commun.*, **47**, 4902 (2011).

[4] (a) J. Schnödt, M. Sieger, B. Sarkar, J. Fiedler, J.S. Manzur, C.Y. Su, W. Kaim. *Z. Anorg. Allg. Chem.*, **637**, 930 (2011); (b) G.B. Li, J.M. Liu, Y.P. Cai, C.Y. Su. *Cryst. Growth Des.*, **11**, 2763 (2011); (c) Q. Zhang, J.Y. Zhang, Q.Y. Yu, M. Pan, C.Y. Su. *Cryst. Growth Des.*, **10**, 4076 (2010).

[5] (a) Y.Y. Liu, J.F. Ma, J. Yang, Z.M. Su. *Inorg. Chem.*, **46**, 3027 (2007); (b) Z.F. Tian, J.G. Lin, Y. Su, L.L. Wen, Y.M. Liu, H.Z. Zhu, Q.J. Meng. *Cryst. Growth Des.*, **7**, 1863 (2007); (c) M. Du, X.J. Jiang, X.J. Zhao. *Inorg. Chem.*, **45**, 3998 (2006); (d) Q. Hua, Y. Zhao, G.C. Xu, M.S. Chen, Z. Su, K. Cai, W.Y. Sun. *Cryst. Growth Des.*, **10**, 2553 (2010).

[6] (a) K.L. Zhang, Y. Chang, C.T. Hou, G.W. Diao, R.T. Wu, S.W. Ng. *CrystEngComm*, **12**, 1194 (2010); (b) K.L. Zhang, C.T. Hou, J.J. Song, Y. Deng, L. Li, S.W. Ng, G.W. Diao. *CrystEngComm*, **14**, 590 (2012); (c) X.P. Li, J.Y. Zhang, M. Pan, S.R. Zheng, Y. Liu, C.Y. Su. *Inorg. Chem.*, **46**, 4617 (2007).

[7] (a) J. Fan, B.E. Hanson. *Inorg. Chem.*, **44**, 6998 (2005); (b) G.C. Xu, Q. Hua, T. Okamura, Z.S. Bai, Y.J. Ding, Y.Q. Huang, G.X. Liu, W.Y. Sun, N. Ueyama. *CrystEngComm*, **11**, 261 (2009).

[8] *SIR92*, A. Altomare, G. Cascarano, C. Giacovazzo, A. Guagliardi, M. Burla, G. Polidori, M. Camalli. *J. Appl. Cryst.*, **27**, 435 (1994).

[9] P.T. Beurskens, G. Admiraal, G. Beurskens, W.P. Bosman, R. de Gelder, R. Israel, J.M.M. Smits. *The DIRFID-99 Program System*, Technical Report of the Crystallography Laboratory, University of Nijmegen, Nijmegen, The Netherlands (1999).

[10] SAINT. *Program for Data Extraction and Reduction*, Bruker AXS, Inc., Madison, WI (2002).

[11] G.M. Sheldrick. *SADABS, Program for Bruker Area Detector Absorption Correction*, University of Göttingen, Göttingen, Germany (1997).

[12] (a) G.M. Sheldrick. *SHELXS-97*, *Programs for Solution of Crystal Structure*, University of Göttingen, Germany (1997); (b) G.M. Sheldrick. *SHELXL-97*, *Programs of Refinement for Crystal Structure*, University of Göttingen, Germany (1997).

[13] (a) A. Kalita, P. Kumar, R.C. Deka, B. Mondal. *Inorg. Chem.*, **50**, 11868 (2011); (b) S. Banthia, A. Samanta. *Inorg. Chem.*, **43**, 6890 (2004). (c) R.D. Willett. *Inorg. Chem.*, **40**, 966 (2001).

[14] (a) G.B. Deacon, R.J. Phillips. *Coord. Chem. Rev.*, **33**, 227 (1980); (b) K. Nakamoto, *Infrared and Raman Spectra of Inorganic and Coordination Compounds*, 4th Edn, p. 231, Wiley, New York (1986).

[15] (a) Z. Su, Z.S. Bai, J. Xu, T. Okamura, G.X. Liu, Q. Chu, X.F. Wang, W.Y. Sun, N. Ueyama. *CrystEngComm*, **11** 873 (2009); (b) Y.Q. Huang, Z.L. Shen, T. Okamura, Y. Wang, X.F. Wang, W.Y. Sun, J.Q. Yu, N. Ueyama. *Dalton Trans.*, 204 (2008).

[16] D. Ghoshal, G. Mostafa, T.K. Maji, E. Zangrando, T.H. Lu, J. Ribas, N.R. Chaudhuri. *New J. Chem.*, **28**, 1204 (2004).

[17] M. Wang, C.B. Ma, H.S. Wang, C.N. Chen, Q.T. Liu. *J. Mol. Struct.*, **873**, 94 (2008).

[18] (a) F. Luo, M.B. Luo, X.L. Tong. *J. Coord. Chem.*, **63**, 1147 (2010); (b) X.L. Wang, J.X. Zhang, G.C. Liu, H.Y. Lin, Z.H. Kang. *J. Coord. Chem.*, **63**, 3933 (2010).